Beyond linear elasticity

Jammed solids at finite shear strain and rate

Boschän, Julia; Vagberg, Daniel; Somfai, Ellák; Tighe, Brian P.

DOI
10.1039/c6sm00536e

Publication date
2016

Document Version
Accepted author manuscript

Published in
Soft Matter

Citation (APA)
Boschän, J., Vagberg, D., Somfai, E., & Tighe, B. P. (2016). Beyond linear elasticity: Jammed solids at finite shear strain and rate. *Soft Matter*, *12*(24), 5450-5460. https://doi.org/10.1039/c6sm00536e

Important note
To cite this publication, please use the final published version (if applicable).
Please check the document version above.

Published in: Soft Matter, 2016, 12, pp. 5450-5460 DOI: 10.1039/C6SM00536E

Beyond linear elasticity: Jammed solids at finite shear strain and rate

Julia Boschan,*[a] Daniel Vågberg,[a] Ellák Somfai,[b] Brian P. Tighe[a]

The shear response of soft solids can be modeled with linear elasticity, provided the forcing is slow and weak. Both of these approximations must break down when the material loses rigidity, such as in foams and emulsions at their (un)jamming point – suggesting that the window of linear elastic response near jamming is exceedingly narrow. Yet precisely when and how this breakdown occurs remains unclear. To answer these questions, we perform computer simulations of stress relaxation and shear start-up tests in athermal soft sphere packings, the canonical model for jamming. By systematically varying the strain amplitude, strain rate, distance to jamming, and system size, we identify characteristic strain and time scales that quantify how and when the window of linear elasticity closes, and relate these scales to changes in the microscopic contact network.

Linear elasticity predicts that when an isotropic solid is sheared, the resulting stress σ is directly proportional to the strain γ and independent of the strain rate $\dot{\gamma}$,

$$\sigma = G_0\gamma\,, \tag{1}$$

with a constant shear modulus G_0.[1] The constitutive relation (1) – a special case of Hooke's law – is a simple, powerful, and widely used model of mechanical response in solids. Yet formally it applies only in the limit of vanishingly slow and weak deformations. In practice materials possess characteristic strain and time scales that define a linear elastic "window", i.e. a parameter range wherein Hooke's law is accurate. Determining the size of this window is especially important in soft solids, where viscous damping and nonlinearity play important roles.[2] The goal of the present work is to determine when Hooke's law holds, and what eventually replaces it, in soft sphere packings close to the (un)jamming transition.

Jammed sphere packings are a widely studied model of emulsions and liquid foams[3–6] and have close connections to granular media and dense suspensions.[7–9] Linear elastic properties of jammed solids, such as moduli and the vibrational density of states, are by now well understood.[10,11] Much less is known about their viscoelastic[7,12] and especially their nonlinear response.[13,14] Yet the jamming transition must determine the linear elastic window, because the shear modulus G_0 vanishes continuously at the jamming point, where the confining pressure p goes to zero. Indeed, studies of oscillatory rheology[15] and shocks[16–18] have shown that, precisely at the jamming point, *any* deformation is effectively fast and strong, and neither viscous effects nor nonlinearities can be neglected.

Because elasticity in foams, emulsions, and other amorphous materials results from repulsive contact forces, microstructural rearrangements of the contact network have signatures in the mechanical response. Namely, they lead to nonlinearity and irreversibility in the particle trajectories, and eventually to steady plastic flow.[19–24] Jammed packings of perfectly rigid particles cannot deform without opening contacts; their response is intrinsically nonlinear, and the number of contact changes per unit strain diverges in the limit of large system size.[25,26] Recently Schreck and co-workers addressed contact changes inside the jammed phase[27–31]; specifically, they asked how many contact changes a jammed packing undergoes before linear response breaks down. They found that trajectories cease to be linear as soon as there is a single rearrangement (made or broken contact) in the contact network, and contact changes occur for vanishing perturbation amplitudes in large systems. Their findings caused the authors to question, if not the formal validity, then at least the usefulness of linear elasticity in jammed solids – not just at the jamming point, but anywhere in the jammed phase.

There is, however, substantial evidence that it is useful to distinguish between linear response in a strict sense, wherein particle trajectories follow from linearizing the equations of motion about an initial condition, and linear response in a weak sense, wherein the stress-strain curve obeys Hooke's law.[32–35] Hooke's law remains applicable close to but above jamming because coarse grained properties are less sensitive to contact changes than are individual trajectories. Agnolin and Roux verified numerically that linearization captures the initial slope of a stress-strain curve, while Van Deen et al. showed explicitly that the slope of the stress-strain curve is on average the same before and after the first contact change[32,33]. Goodrich et al. further demonstrated that contact changes have negligible effect on the density of states.[35] These results verify the intuitive expectation that weak linear response remains valid even after strict linear response is violated. This in turn raises – but does not answer – the question of when Hooke's law eventually does break down.

[a] *Delft University of Technology, Process & Energy Laboratory, Leeghwaterstraat 39, 2628 CB Delft, The Netherlands; E-mail: j.boschan@tudelft.nl*
[b] *Institute for Solid State Physics and Optics, Wigner Research Center for Physics, Hungarian Academy of Sciences, P.O. Box 49, H-1525 Budapest, Hungary*

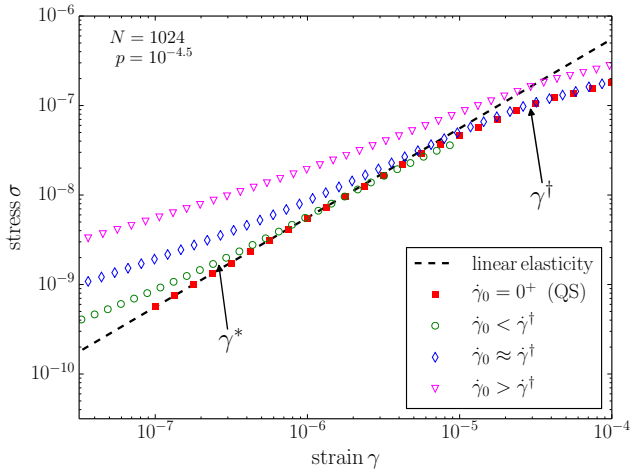

Fig. 1 Ensemble-averaged stress-strain curves of packings sheared at varying strain rate $\dot\gamma_0$. Close to the jamming point the linear stress-strain curve (dashed line) predicted by Hooke's law holds over a narrow interval at low strain, with deviations due to viscous and plastic dissipation. The crossover strains γ^* and $\gamma^\dagger$ are indicated for the data sheared at slow but finite rate $0 < \dot\gamma_0 < \dot\gamma^\dagger$ (open circles).

Recent experiments [13,21], simulations, [14,24,36,37] and theory [38] provide evidence for a two stage yielding process, where response first becomes nonlinear (stress is no longer directly proportional to strain) and only later establishes steady plastic flow (stress is independent of strain). To distinguish these two crossovers, we will refer to them as softening and yielding, respectively; our focus will be mainly on the softening crossover. It remains unclear precisely how rate dependence, nonlinearity, and contact changes contribute to the breakdown of linear elasticity and onset of softening. In order to unravel these effects, it is necessary to vary strain, strain rate, pressure, and system size simultaneously and systematically – as we do here for the first time. Using simulations of viscous soft spheres, we find that Hooke's law is valid within a surprisingly narrow window bounded by viscous dissipation at small strain and plastic dissipation at large strain. The size of the linear elastic window displays power law scaling with pressure and correlates with the accumulation of not one, but an extensive number of contact changes.

The basic scenario we identify is illustrated in Fig. 1, which presents ensemble-averaged shear stress versus strain. Shear is applied via a constant strain rate $\dot\gamma_0$ at fixed volume. We identify three characteristic scales, each of which depend on the initial pressure p: (i) For strains below $\gamma^* \equiv \dot\gamma_0 \tau^*$, where τ^* is a diverging time scale, viscous stresses are significant and Eq. (1) underestimates the stress needed to deform the material. This crossover strain vanishes under quasistatic shear ($\dot\gamma_0 \to 0$, filled squares). (ii) Above a vanishing strain $\gamma^\dagger$ the material softens and Hooke's law overestimates the stress. This crossover is rate-independent, consistent with plastic effects. (iii) For strain rates above a vanishing scale $\dot\gamma^\dagger$ (triangles), Eq. (1) is never accurate and there is no strain interval wherein the material responds as a linear elastic solid.

1 Soft spheres: Model and background

We first introduce the soft sphere model and summarize prior results regarding linear elasticity near jamming.

1.1 Model

We perform numerical simulations of the Durian bubble model [4], a mesoscopic model for wet foams and emulsions. The model treats bubbles/droplets as non-Brownian disks that interact via elastic and viscous forces when they overlap. Elastic forces are expressed in terms of the overlap $\delta_{ij} = 1 - r_{ij}/(R_i + R_j)$, where R_i and R_j denote radii and $\vec r_{ij}$ points from the center of particle i to the center of j. The force is repulsive and acts along the unit vector $\hat r_{ij} = \vec r_{ij}/r_{ij}$:

$$\vec f_{ij}^{\,\mathrm{el}} = \begin{cases} -k(\delta_{ij})\,\delta_{ij}\,\hat r_{ij}\,, & \delta_{ij} > 0 \\ \vec 0, & \delta_{ij} < 0. \end{cases} \tag{2}$$

The prefactor k is the contact stiffness, which generally depends on the overlap

$$k = k_0\,\delta^{\alpha-2}\,. \tag{3}$$

Here k_0 is a constant and α is an exponent parameterizing the interaction. In the following we consider harmonic interactions ($\alpha = 2$), which provide a reasonable model for bubbles and droplets that resist deformation due to surface tension; we also treat Hertzian interactions ($\alpha = 5/2$), which correspond to elastic spheres.

We perform simulations using two separate numerical methods. The first is a molecular dynamics (MD) algorithm that implements SLLOD dynamics [39] using the velocity-Verlet scheme. Energy is dissipated by viscous forces that are proportional to the relative velocity $\Delta\vec v_{ij}^{\,c}$ of neighboring particles evaluated at the contact,

$$\vec f_{ij}^{\,\mathrm{visc}} = -\tau_0\,k(\delta_{ij})\,\Delta\vec v_{ij}^{\,c}\,, \tag{4}$$

where τ_0 is a microscopic relaxation time. Viscous forces can apply torques, hence particles are allowed to rotate as well as translate.

In addition to MD, we also perform simulations using a nonlinear conjugate gradient (CG) routine [40], which keeps the system at a local minimum of the potential energy landscape, which itself changes as the system undergoes shearing. The

dynamics are therefore quasistatic, i.e. the particle trajectories correspond to the limit of vanishing strain rate.

All results are reported in units where k_0, τ_0, and the average particle diameter have all been set to one. Each disk is assigned a uniform mass $m_i = \pi R_i^2$, which places our results in the overdamped limit.

Bubble packings consist of $N = 128$ to 2048 disks in the widely studied 50:50 bidisperse mixture with a 1.4:1 diameter ratio.[41] Shear is implemented via Lees-Edwards "sliding brick" boundary conditions at fixed volume V (area in two dimensions). The stress tensor is given by

$$\sigma_{\alpha\beta} = \frac{1}{2V}\sum_{ij} f_{ij,\alpha} r_{ij,\beta} - \frac{1}{V}\sum_{i} m_i v_{i,\alpha} v_{i,\beta}\,, \qquad (5)$$

where $\vec{f}_{ij}$ is the sum of elastic and viscous contact forces acting on particle i due to particle j, and $\vec{v}_i$ is the velocity of particle i. Greek indices label components along the Cartesian coordinates x and y. The confining pressure is $p = -(1/D)(\sigma_{xx} + \sigma_{yy})$, where $D = 2$ is the spatial dimension, while the shear stress is $\sigma = \sigma_{xy}$. The second term on the righthand side of Eq. (5) is a kinetic stress, which is always negligible in the parameter ranges investigated here.

We use the pressure p to measure a packing's distance to jamming. Common alternatives are the excess volume fraction $\Delta\phi = \phi - \phi_c$ and excess mean contact number $\Delta z = z - z_c$, where ϕ_c and $z_c = 2D$ refer to the respective values at jamming.[10,42,43] We prefer to use the pressure as an order parameter because it is easily accessed in experiments (unlike z), and its value at the transition, $p_c = 0$, is known exactly (unlike ϕ). Therefore, prior to shearing, all packings are prepared at a targeted pressure. The equilibration procedure includes the box size and shape in addition to the particle positions as degrees of freedom, which guarantees that the stress tensor is proportional to the unit matrix and that the packing is stable to shear perturbations.[44] At each pressure there are fluctuations in ϕ and z, however for a given preparation protocol the probability distributions of ϕ and z tend to a delta function with increasing N[40,42], and typical values (e.g. the mean or mode) satisfy the scaling relation

$$\frac{p}{k} \sim \Delta\phi \sim \Delta z^2\,. \qquad (6)$$

Here k is a typical value of the contact stiffness $k(\delta_{ij})$ in Eq. (3), which is simply the constant k_0 in the harmonic case ($\alpha = 2$). For other values of α, however, k depends on the pressure. As the typical force trivially reflects its bulk counterpart, $f \sim p$, the contact stiffness scales as $k \sim f/\delta \sim p^{(\alpha-2)/(\alpha-1)}$. In the following, all scaling relations will specify their dependence on k and the time scale τ_0. In the present work τ_0 is independent of the overlap between particles (as in the viscoelastic Hertzian contact problem[45]), but we include

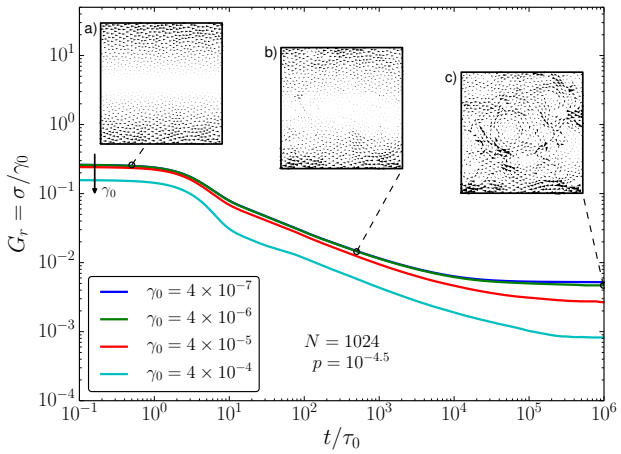

Fig. 2 The ensemble-averaged relaxation modulus G_r at pressure $p = 10^{-4.5}$ for four values of the strain amplitude γ_0. In all four cases, G_r displays an initial plateau corresponding to affine particle motion (inset a), followed by a power law decay as the particle displacements become increasingly non-affine (b). At long times the stress is fully relaxed and the final particle displacements are strongly non-affine (c).

τ_0 because one could imagine a damping coefficient $k\tau_0$ with more general overlap dependence than the form treated here.

1.2 Shear modulus and the role of contact changes

In large systems the linear elastic shear modulus G_0 vanishes continuously with pressure,

$$G_0/k \sim (p/k)^{\mu}\,, \qquad (7)$$

with $\mu = 1/2$. Hence jammed solids' shear stiffness can be arbitrarily weak. The scaling of G_0 has been determined multiple times, both numerically[42,46,47] and theoretically[15,48,49]; it is verified for our own packings in Fig. 3a and c, as discussed in Section 2.

There are two standard approaches to determining G_0. The first, which we employ, is to numerically impose a small but finite shear strain and relax the packing to its new energy minimum.[42,46] In the second approach one writes down the D equations of motion for each particle and linearizes them about a reference state, which results in a matrix equation involving the Hessian; solutions to this equation describe the response to an infinitesimally weak shear.[15,44,47,49–51] The latter approach allows access to the zero strain limit, but it is blind to any influence of contact changes.

When calculating the shear modulus using the finite difference method over strain differences as small as 10^{-9}, double precision arithmetic does not provide sufficiently accurate re-

sults.[52] A straightforward but computationally expensive approach is to switch to quadruple precision. Instead we represent each particle position as the sum of two double precision variables, which gives sufficient precision for the present work and is significantly faster than the GCC Quad-Precision Math Library. Since we are aware of precision issues, we have taken great care to verify our results. The shear modulus calculated using finite difference method agrees with the corresponding shear modulus obtained using the Hessian matrix[10], provided the strain amplitude is small enough that the packing neither forms new contacts, nor breaks existing ones.

Van Deen et al.[33] measured the typical strain at the first contact change, and found that it depends on both pressure and system size,

$$\gamma_{\rm cc}^{(1)} \sim \frac{(p/k)^{1/2}}{N}\,. \tag{8}$$

The inverse N-dependence is consistent with what one would expect from a Poisson process. Similar to the findings of Schreck et al.[27], who determined a critical perturbation amplitude by deforming packings along normal modes, the strain scale in Eq. (8) vanishes in the large system limit, even at finite pressure. Earlier work by Combe and Roux probed deformations of rigid disks precisely at jamming; they identified a dimensionless stress scale $\sigma_{\rm cc}^{(1)}/p \sim 1/N^{1.16}$. Naïvely extrapolating to soft spheres would then give a strain scale $\gamma_{\rm cc}^{(1)} \sim \sigma_{\rm cc}^{(1)}/G_0 \sim (p/k)^{1/2}/N^{1.16}$, in reasonable but not exact agreement with Eq. (8).

2 Stress relaxation

We will characterize mechanical response in jammed solids using stress relaxation and flow start-up tests, two standard rheological tests. In the linear regime they are equivalent to each other and to other common tests such as creep response and oscillatory rheology, because complete knowledge of the results of one test permits calculation of the others.[2]

We employ stress relaxation tests to access the time scale τ^* over which viscous effects are significant, and we use flow start-up tests to determine the strain scale $\gamma^\dagger$ beyond which the stress-strain curve becomes nonlinear. We consider stress relaxation first.

In a stress relaxation test one measures the time-dependent stress $\sigma(t,\gamma_0)$ that develops in a response to a sudden shear strain with amplitude γ_0, i.e.

$$\gamma(t) = \begin{cases} 0 & t<0 \\ \gamma_0 & t \geq 0\,. \end{cases} \tag{9}$$

The relaxation modulus is

$$G_r(t,\gamma_0) \equiv \frac{\sigma(t,\gamma_0)}{\gamma_0}\,. \tag{10}$$

We determine G_r by employing the shear protocol of Hatano.[7] A packing's particles and simulation cell are affinely displaced in accordance with a simple shear with amplitude γ_0. E.g. for a simple shear in the $\hat{x}$-direction, the position of a particle i initially at (x_i, y_i) instantaneously becomes $(x_i + \gamma_0 y_i, y_i)$, while the Lees-Edwards boundary conditions are shifted by $\hat{\gamma}_0 L_y$, where L_y is the height of the simulation cell. Then the particles are allowed to relax to a new mechanical equilibrium while the Lees-Edwards offset is held fixed.

The main panel of Fig. 2 illustrates four relaxation moduli of a single packing equilibrated at pressure $p = 10^{-4.5}$ and then sheared with strain amplitudes varying over three decades. All four undergo a relaxation from an initial plateau at short times to a final, lower plateau at long times. The character of the particle motions changes as relaxation progresses in time. While the particle motions immediately after the deformation are affine (Fig. 2a), they become increasingly non-affine as the stresses relax to a new static equilibrium (Fig. 2b,c).

For sufficiently small strain amplitudes, linear response is obtained and any dependence of the relaxation modulus on γ_0 is sub-dominant. The near-perfect overlap of the moduli for the two smaller strain amplitudes Fig. 2 indicates that they reside in the linear regime. The long-time plateau is then equal to the linear elastic modulus G_0. In practice there is a crossover time scale τ^* such that for longer times $t \gg \tau^*$ viscous damping is negligible and the relaxation modulus is well approximated by its asymptote, $G_r \simeq G_0$. For the data in Fig. 2a the crossover time is $\tau^* \approx 10^4 \tau_0$. In the following Section we will determine the scaling of τ^* with pressure.

2.1 Scaling in the relaxation modulus

We now characterize stress relaxation in linear response by measuring the relaxation modulus, averaged over ensembles of packings prepared at varying pressure. We will show that G_r collapses to a critical scaling function governed by the distance to the jamming point, thereby providing a numerical test of recent theoretical predictions by Tighe.[15] In particular we test the prediction that the rescaled shear modulus G/G_0 collapses to a master curve when plotted versus the rescaled time t/τ^*, with a relaxation time that diverges as

$$\tau^* \sim \left(\frac{k}{p}\right)^{\lambda} \tau_0 \tag{11}$$

for $\lambda = 1$. Both the form of the master curve and the divergence of the relaxation time can be related to slowly relaxing eigenmodes that become increasingly abundant on approach to jamming. These modes favor sliding motion between contacting particles[47], reminiscent of zero energy floppy modes[53], and play an important role in theoretical de-

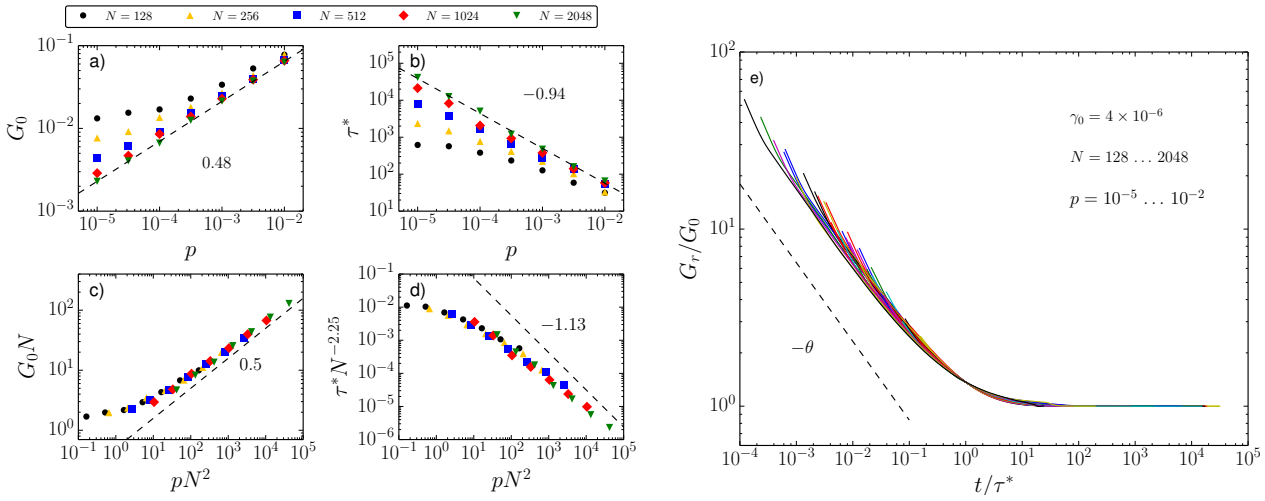

Fig. 3 (a) The linear shear modulus G_0 in harmonic packings for varying pressure p and number of particles N. (b) The relaxation time τ^* for the same range of p and N as in (a). (c) Finite size scaling collapse of G_0. (d) Finite size scaling collapse of τ^*. (e) The relaxation modulus G_r collapses to a master curve when G_r and t are rescaled with G_0 and τ^*, respectively, as determined in (a) and (b). At short times the master curve decays as a power law with exponent $\theta = \mu/\lambda \approx 0.44$ (dashed line), using the estimates from (c) and (d).

scriptions of mechanical response near jamming.[15,48,49,51,54] For further details, we direct the reader to Ref.[15].

We showed in Fig. 2 that a packing relaxes in three stages. The short-time plateau is trivial, in the sense that viscous forces prevent the particles from relaxing at rates faster than $1/\tau_0$; hence particles have not had time to depart significantly from the imposed affine deformation and the relaxation modulus reflects the contact stiffness, $G_r \sim k$. We therefore focus hereafter on the response on time scales $t \gg \tau_0$.

To demonstrate dynamic critical scaling in G_r, we first determine the scaling of its long-time asymptote G_0. We then identify the time scale τ^* on which G_r significantly deviates from G_0. Finally, we show that rescaling with these two parameters collapses the relaxation moduli for a range of pressures to a single master curve. While we address variations with strain in subsequent Sections, the strain amplitude here is fixed to a value $\gamma_0 = 10^{-5.5}$. We have verified that this strain amplitude is in the linear regime for all of the data presented in this Section.

As noted above, at long times the relaxation modulus approaches the linear quasistatic modulus, $G_r(t \to \infty) \simeq G_0$. We verify Eq. (7) in our harmonic packings with two closely related tests. First we fit a power law to data from systems of $N = 2048$ particles; the best fit has a slope of 0.48 (Fig. 3a, dashed line). Next, we repeat the finite size scaling analysis of Goodrich et al.[55], who showed that finite size effects become important when a packing has $O(1)$ contacts in excess of isostaticity, or equivalently when $p/k \sim 1/N^2$ – c.f. Eq. (6). Consistent with their results, Fig. 3a shows clear finite size effects in G_0. Data for different system sizes can be collapsed to a master curve by plotting $\mathcal{G} \equiv G_0 N$ versus the rescaled pressure $x \equiv pN^2$. The master curve approaches a power law x^μ consistent with $\mu = 0.5$, as shown in Fig. 3c. The scaling of Eq. (7), and specifically the value $\mu = 1/2$, is verified by this data collapse, together with the requirement for the modulus to be an intensive property of large systems. To see this, note that G_0 is intensive only if $\mathcal{G} \sim x^{1/2}$ for large x.

Again referring to Fig. 2, there is clearly some time scale τ^* such that for $t < \tau^*$ the relaxation modulus deviates significantly from the quasistatic modulus. The relaxation time is determined from the point where G_r, averaged over an ensemble of at least 100 packings per condition, has decayed to within a fraction Δ of its final value, $G_r(t = \tau^*) = (1 + \Delta)G_0$. We present data for $\Delta = 1/e$, but similar scaling results for a range of Δ.[37] Raw data for varying p and N is shown in Fig. 3b. Fitting a power law to the data for $N = 2048$ gives an exponent $\lambda = 0.94$. We now again seek to refine our estimate by collapsing data to a master curve. As τ^* and G_0 are both properties of the relaxation modulus, we require the rescaled pressure to remain $x = pN^2$, which collapses the G_0 data. We then search for data collapse in τ^* by rescaling the relaxation time as $\tau^*/N^{2\lambda}$, which implies that τ^* diverges in large systems in accord with Eq. (11). While we find reasonable data collapse for $\lambda = 0.94$, the best collapse occurs for a larger value $\lambda \approx 1.13$, shown in Fig. 3d. The theoretical prediction $\lambda = 1$ clearly falls within the range of our numerical estimates,[15] although on the basis of the present data we cannot exclude a slightly different value of λ.

We now use the linear quasistatic modulus G_0 and the characteristic time scale τ^* to collapse the relaxation modulus to a

master curve $\mathcal{R}(s)$. Fig. 3c plots $\mathcal{R} \equiv G_r/G_0$ versus $s \equiv t/\tau^*$ for a range of pressures and system sizes; data from the trivial affine regime at times $t < 10\tau_0$ have been excluded. The resulting data collapse is excellent, and the master curve it reveals has two scaling regimes: $\mathcal{R} \simeq 1$ for $s \gg 1$, and $\mathcal{R} \sim s^{-\theta}$ for $s \ll 1$. The plateau at large s corresponds to the quasistatic scaling $G_r \simeq G_0$. The power law relaxation at shorter times corresponds to $G_r \sim G_0(t/\tau^*)^{-\theta}$ for some exponent θ. By considering a marginal solid prepared at the jamming point, one finds that the prefactor of $t^{-\theta}$ cannot depend on the pressure. Invoking the pressure scaling of G_0 and τ^* in the large N limit, identified above, we conclude that $\theta = \mu/\lambda$. Hence in large systems the relaxation modulus scales as

$$\frac{G_r(t)}{k} \sim \begin{cases} (\tau_0/t)^{\theta} & 1 \ll t/\tau_0 \ll (k/p)^{\lambda} \\ (p/k)^{\mu} & (k/p)^{\lambda} \ll t/\tau_0 \,. \end{cases} \tag{12}$$

with $\mu = 1/2$, $\lambda \approx 1$, and $\theta = \mu/\lambda \approx 0.5$. These findings are consistent with the theoretical predictions in Ref.[15].

Anomalous stress relaxation with exponent $\theta \approx 0.5$ was first observed in simulations below jamming[7] and is also found in disordered spring networks.[56,57] It is related via Fourier transform to the anomalous scaling of the frequency dependent complex shear modulus $G^* \sim (\imath\omega)^{1-\theta}$ found in viscoelastic solids near jamming.[15] We revisit the scaling relation of Eq. (12) in Section 3.6.

3 Finite strain

When does linear elasticity break down under increasing strain, and what lies beyond? To answer these questions, we now probe shear response at finite strain using flow start-up tests.

3.1 Flow start-up

In a flow start-up test, strain-controlled boundary conditions are used to "turn on" a flow with constant strain rate $\dot\gamma_0$ at time $t = 0$, i.e.

$$\gamma(t) = \begin{cases} 0 & t < 0 \\ \dot\gamma_0 t & t \geq 0 \end{cases} \tag{13}$$

To implement flow start-up in MD, at time $t = 0$ a packing's particles and simulation cell are instantaneously assigned an affine velocity profile $\vec v_i = (\dot\gamma_0\, y_i, 0)^T$ in accordance with a simple shear with strain rate $\dot\gamma_0$; the Lees-Edwards images of the simulation cell are assigned a commensurate velocity. Then the particles are allowed to evolve according to Newton's laws while the Lees-Edwards boundary conditions maintain constant velocity, so that the total strain $\gamma(t)$ grows linearly in time.

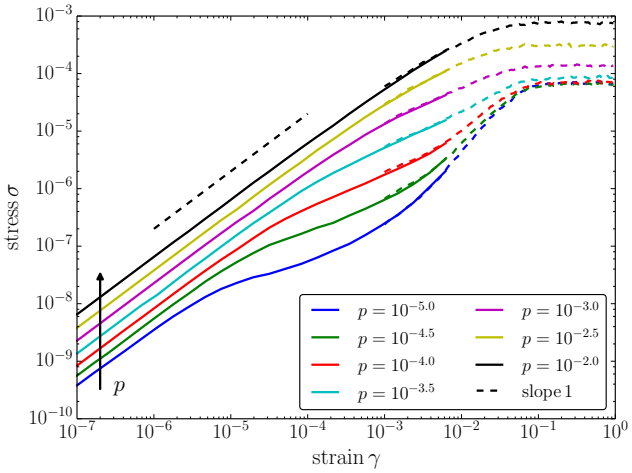

Fig. 4 Averaged stress-strain curves under quasistatic shear at varying pressure p. Solid and dashed curves were calculated using different strain protocols. Dashed curves: fixed strain steps of 10^{-3}, sheared to a final strain of unity. Solid curves: logarithmically increasing strain steps, beginning at 10^{-9} and reaching a total strain of 10^{-2} after 600 steps.

We also perform quasistatic shear simulations using nonlinear CG minimization to realize the limit of vanishing strain rate. Particle positions are evolved by giving the Lees-Edwards boundary conditions a series of small strain increments and equilibrating to a new minimum of the elastic potential energy. The stress σ is then reported as a function of the accumulated strain. For some runs we use a variable step size in order to more accurately determine the response at small strain.

Fig. 1 illustrates the output of both the finite strain rate and quasistatic protocols.

3.2 Quasistatic stress-strain curves

To avoid complications due to rate-dependence, we consider the limit of vanishing strain rate first.

Fig. 4 plots the ensemble-averaged stress-strain curve $\sigma(\gamma)$ for harmonic packings at varying pressure. Packings contain $N = 1024$ particles, and each data point is averaged over at least 600 configurations. Several features of the stress-strain curves stand out. First, there is indeed a window of initially linear growth. Second, beyond a strain of approximately 5 - 10% the system achieves steady plastic flow and the stress-strain curve is flat. Finally, the end of linear elasticity and the beginning of steady plastic flow do not generally coincide; instead there is an interval in which the stress-strain curve has a complex nonlinear form. We shall refer to the end of the linear elastic regime as "softening" because the stress initially dips *below* the extrapolation of Hooke's law. (In the plastic-

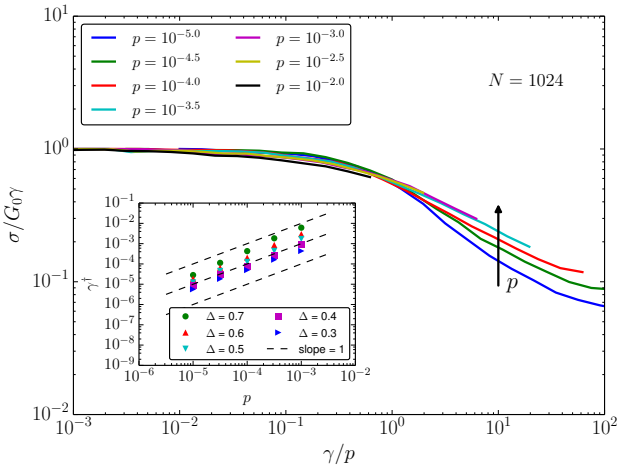

Fig. 5 (main panel) Data from Fig. 4, expressed as a dimensionless effective shear modulus $\sigma/G_0\gamma$ and plotted versus the rescaled strain γ/p. (inset) The crossover strain $\gamma^\dagger$ where the effective shear modulus has decayed by an amount Δ in a system of $N = 1024$ particles.

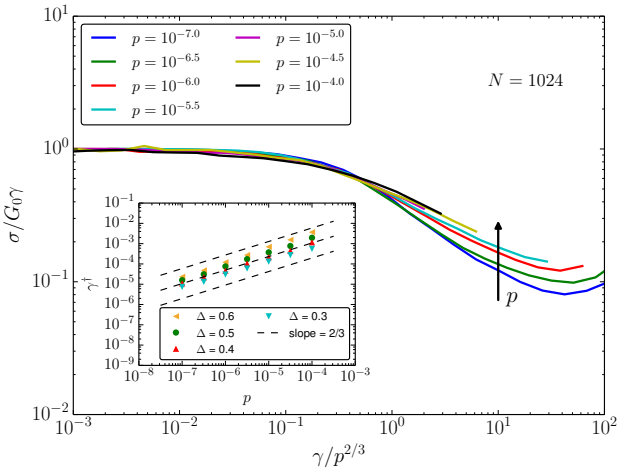

Fig. 6 (main panel) The dimensionless shear modulus of quasistatically sheared Hertzian packings plotted versus the rescaled strain $\gamma/p^{2/3}$. (inset) Pressure-dependence of the crossover strain $\gamma^\dagger$.

ity literature the same phenomenon would be denoted "strain hardening".) Moreover, for sufficiently low pressures there is a strain interval over which the stress increases faster than linearly. This surprising behavior is worthy of further attention, but the focus of the present work will be on the end of linear elasticity and the onset of softening. This occurs on a strain scale $\gamma^\dagger$ that clearly depends on pressure.

3.3 Onset of softening

We now determine the pressure and system size dependence of the softening (or nonlinear) strain scale $\gamma^\dagger$.

Fig. 5 replots the quasistatic shear data from Fig. 4 (solid curves), now with the linear elastic trend $G_0\gamma$ scaled out. The rescaling collapses data for varying pressures in the linear regime and renders the linear regime flat. The strain axis in Fig. 5b is also rescaled with the pressure, a choice that will be justified below. The onset of softening occurs near unity in the rescaled strain coordinate for all pressures, which suggests that $\gamma^\dagger$ scales linearly with p in harmonic packings ($\alpha = 2$).

Unlike the linear relaxation modulus in Fig. 3c, the quasistatic shear data in Fig. 5 do not collapse to a master curve; instead the slope immediately after softening steepens (in a log-log plot) as the pressure decreases. As a result, it is not possible to unambiguously identify a correlation $\gamma^\dagger \sim p^\nu$ between the crossover strain and the pressure. To clarify this point, the inset of Fig. 5 plots the strain where $\sigma/G_0\gamma$ has decayed by an amount Δ from its plateau value, denoted $\gamma^\dagger(\Delta)$. This strain scale is indeed approximately linear in the pressure p (dashed curves), but a power law fit gives an exponent ν in the range 0.87 to 1.06, depending on the value of Δ. Bearing the above subtlety in mind, we nevertheless conclude that an effective power law with $\nu = 1$ provides a reasonable description of the softening strain. Section 2.1 presents further evidence to support this conclusion.

3.4 Hertzian packings

In the previous section the pressure-dependence of $\gamma^\dagger$ was determined for harmonic packings. We now generalize this result to other pair potentials, with numerical verification for the case of Hertzian packings ($\alpha = 5/2$).

Recall that the natural units of stress are set by the contact stiffness k, which itself varies with pressure when $\alpha \neq 2$. Based on the linear scaling of $\gamma^\dagger$ in harmonic packings, we anticipate

$$\gamma^\dagger \sim \frac{p}{k} \sim p^{1/(\alpha-1)}\,, \qquad (14)$$

which becomes $\gamma^\dagger \sim p^{2/3}$ in the Hertzian case. To test this relation, we repeat the analysis of the preceding Section; results are shown in Fig. 6. We again find a finite linear elastic window that gives way to softening. Softening onset can again be described with a Δ-dependent exponent (see inset). Its value has a narrow spread about $2/3$; power law fits give slopes between 0.63 and 0.74.

3.5 Relating softening and contact changes

Why does the linear elastic window close when it does? We now seek to relate softening with contact changes on the particle scale.[21–24,27,33] Specifically, we identify a correlation be-

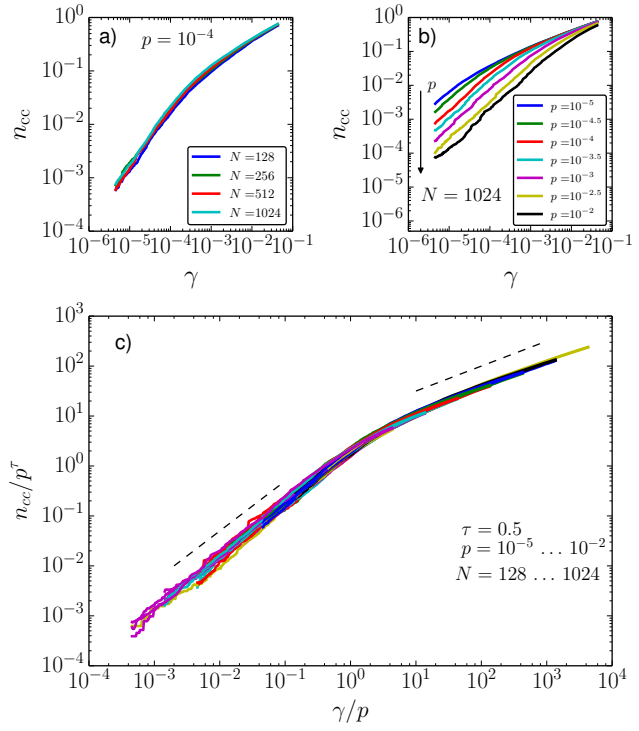

Fig. 7 The contact change density shown for (a) varying system size and (b) varying pressure. (c) Data collapse for pressures $p = 10^{-2} \ldots 10^{-5}$ in half decade steps and system sizes $N = 128 \ldots 1024$ in multiples of 2. Dashed lines indicate slopes of 1 and 1/2.

tween the softening strain $\gamma^\dagger$, the cumulative number of contact changes, and the distance to the isostatic contact number z_c. In so doing we will answer the question first posed by Schreck and co-workers[27], who asked how many contact changes a packing can accumulate while still displaying linear elastic response.

We begin by investigating the ensemble-averaged contact change density $n_{\rm cc}(\gamma) \equiv [N_{\rm make}(\gamma) + N_{\rm break}(\gamma)]/N$, where $N_{\rm make}$ and $N_{\rm break}$ are the number of made and broken contacts, respectively, accumulated during a strain γ. Contact changes are identified by comparing the contact network at strain γ to the network at zero strain.

In Fig. 7a we plot $n_{\rm cc}$ for packings of harmonic particles at pressure $p = 10^{-4}$ and varying system size. The data collapse to a single curve, indicating that $n_{\rm cc}$ is indeed an intensive quantity. The effect of varying pressure is shown in Fig. 7b. There are two qualitatively distinct regimes in $n_{\rm cc}$, with a crossover governed by pressure.

To better understand these features, we seek to collapse the $n_{\rm cc}$ data to a master curve. By plotting $\mathcal{N} \equiv n_{\rm cc}/p^\tau$ versus $y \equiv \gamma/p$, we obtain excellent collapse for $\tau = 1/2$, as shown in Fig. 7b for the same pressures as in Fig. 7a and system sizes $N = 128 \ldots 1024$. The scaling function $\mathcal{N} \sim y$ for small y, while $\mathcal{N} \sim y^\tau$ for $y \gtrsim 1$. The rescaled strain y provides further evidence for a crossover scale $\gamma^\dagger \sim p/k$, now apparent at the microscale. Moreover, the fact that data for varying system sizes all collapse to the same master curve is an important indicator that $\gamma^\dagger$ is an intensive strain scale that remains finite in the large system size limit.

The scaling collapse in Fig. 7c generalizes the results of Van Deen et al.[33], who determined the strain scale $\gamma_{\rm cc}^{(1)} \sim (p/k)^{1/2}/N$ associated with the first contact change. To see this, note that the inverse slope $({\rm d}\gamma/{\rm d}n_{\rm cc})/N$ represents the average strain interval between contact changes at a given strain. Hence the initial slope of $n_{\rm cc}$ is fixed by $\gamma_{\rm cc}^{(1)}$,

$$n_{\rm cc}(\gamma) \simeq \frac{1}{N}\left(\frac{\gamma}{\gamma_{\rm cc}^{(1)}}\right) \qquad (15)$$

as $\gamma \to 0$. From Fig. 7 it is apparent that $n_{\rm cc}$ remains linear in γ up to the crossover strain $\gamma^\dagger$. We conclude that $\gamma_{\rm cc}^{(1)}$ describes the strain between successive contact changes over the entire interval $0 < \gamma < \gamma^\dagger$. In the softening regime the strain between contact changes increases; it scales as $n_{\rm cc} \sim \gamma^{1/2}$ (see Fig. 7c). This corresponds to an increasing and strain-dependent mean interval $\gamma^{1/2}/N$ between contact changes.

Let us now re-interpret the softening crossover strain $\gamma^\dagger \sim \Delta z^2$ (c.f. Eq. (6)) in terms of the coordination of the contact network. We recall that $\Delta z = z - z_c$ is the difference between the initial contact number z and the isostatic value z_c, which corresponds to the minimum number of contacts per particle needed for rigidity. The excess coordination Δz is therefore an important characterization of the contact network. The contact change density at the softening crossover, $n_{\rm cc}^\dagger$, can be related to Δz via Eq. (15), while making use of Eq. (6),

$$n_{\rm cc}^\dagger \equiv n_{\rm cc}(\gamma^\dagger) \sim \Delta z\,. \qquad (16)$$

Hence we have empirically identified a topological criterion for the onset of softening: an initially isotropic packing softens when it has undergone an extensive number of contact changes that is comparable to the number of contacts it initially had in excess of isostaticity. Note that this does not mean the packing is isostatic at the softening crossover, as $n_{\rm cc}$ counts both made and broken contacts.

3.6 Rate-dependence

To this point we have considered nonlinear response exclusively in the limit of quasistatic shearing. A material accumulates strain quasistatically when the imposed strain rate is slower than the longest relaxation time in the system. Because relaxation times near jamming are long and deformations in the lab always occur at finite rate, we can anticipate

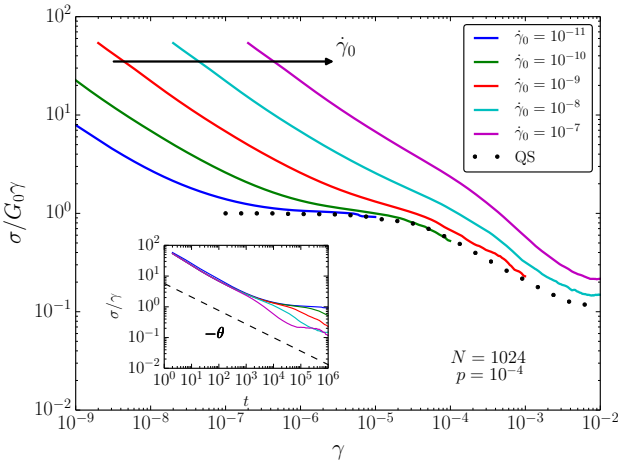

Fig. 8 The effective shear modulus during flow start-up for packings of $N = 1024$ particles at pressure $p = 10^{-4}$, plotted versus strain for varying strain rates $\dot\gamma_0$. (inset) The same data collapses for early times when plotted versus t, decaying as a power law with exponent $\theta = \mu/\lambda \approx 0.44$ (dashed line).

that quasistatic response is difficult to achieve and that rate-dependence generically plays a significant role. Hence it is important to consider shear at finite strain and finite strain rate. We now consider flow start-up tests in which a finite strain rate $\dot\gamma_0$ is imposed at time $t = 0$, cf. Eq. (13).

Fig. 8 displays the mechanical response to flow start-up for varying strain rates. To facilitate comparison with the quasistatic results of the previous section, data are plotted in terms of the dimensionless quantity $\sigma(t;\dot\gamma_0)/G_0\gamma$, which we shall refer to as the effective shear modulus. The data are for systems of $N = 1024$ particles, averaged over an ensemble of around 100 realizations each. Here we plot data for the pressure $p = 10^{-4}$; results are qualitatively similar for other pressures. For comparison, we also plot the result of quasistatic shear (solid circles) applied to the same ensemble of packings.

Packings sheared sufficiently slowly follow the quasistatic curve; see e.g. data for $\dot\gamma_0 = 10^{-11}$. For smaller strains, however, the effective shear modulus is stiffer than the quasistatic curve and decays as $\sigma/\gamma \sim t^{-\theta}$ (see inset). This is rate-dependence: for a given strain amplitude, the modulus increases with increasing strain rate. Correspondingly, the characteristic strain γ^* where curves in the main panel of Fig. 8 reach the linear elastic plateau ($\sigma/G_0\gamma \approx 1$) grows with $\dot\gamma_0$. For sufficiently high strain rates there is no linear elastic plateau; for the data in Fig. 8 this occurs for $\dot\gamma_0 \approx 10^{-8}$. Hence there is a characteristic strain rate, $\dot\gamma^\dagger$, beyond which the linear elastic window has closed: packings sheared faster than $\dot\gamma^\dagger$ are always rate-dependent and/or strain softening.

To understand the rate-dependent response at small strains, we revisit the relaxation modulus determined in Section 2. In linear response the stress after flow start-up depends only on the elapsed time $t = \gamma/\dot\gamma_0$,

$$\frac{\sigma}{\gamma} = \frac{1}{t}\int_0^t G_r(t')\,\mathrm{d}t' \,. \tag{17}$$

Employing the scaling relations of Eq. (12), one finds

$$\frac{\sigma}{\gamma} \sim k\left(\frac{\tau_0}{t}\right)^\theta , \qquad \tau_0 < t < \tau^* , \tag{18}$$

as verified in Fig. 8 (inset). Linear elasticity $\sigma/\gamma \simeq G_0$ is only established at longer times, when $\gamma > \dot\gamma_0\tau^* \sim (k/p)^\lambda\,\dot\gamma_0\tau_0$. Hence the relaxation time τ^* plays an important role: it governs the crossover from rate-dependent to quasistatic linear response. The system requires a time τ^* to relax after a perturbation. When it is driven at a faster rate, it cannot relax fully and hence its response depends on the driving rate.

We can now identify the characteristic strain rate $\dot\gamma^\dagger$ where the linear elastic window closes. This rate is reached when the bound on quasistaticity, $\gamma > \dot\gamma_0\tau^*$, collides with the bound on linearity, $\gamma < \gamma^\dagger$, giving

$$\dot\gamma^\dagger \sim \frac{(p/k)^{1+\lambda}}{\tau_0} , \tag{19}$$

with $1 + \lambda \approx 2$. This strain rate vanishes rapidly near jamming, hence packings must be sheared increasingly slowly to observe a stress-strain curve that obeys Hooke's law.

4 Implications for experiment

The time scale τ^*, strain scales γ^* and $\gamma^\dagger$, and strain rate $\dot\gamma^\dagger$ all place bounds on the window of linear elastic response. Which of these quantities are most relevant depends on the particular rheological test one performs. For example, in a flow start-up test Hooke's Law is accurate within the window $\gamma^* < \gamma < \gamma^\dagger$, provided the strain rate $\dot\gamma_0 < \dot\gamma^\dagger$. This is the scenario depicted in Fig. 1; it is also illustrated schematically in Fig. 9. In a stress relaxation test, however, the strain amplitude and test duration can be varied independently. Hooke's law is then accurate for $\gamma_0 < \gamma^\dagger$ provided one waits for a time $t > \tau^*$ for the system to relax. (We have verified that the softening onset still occurs at $\gamma^\dagger$ when the full strain γ_0 is applied in one step, as opposed to a quasistatic series of small steps.) Similar parameter ranges can be constructed for other rheological tests.

What experimental scales do these quantities correspond to? Most importantly, one must collect data in the scaling regime near jamming. Quantities such as the excess coordination and moduli show gradual deviations from scaling when the excess volume fraction exceeds $\Delta\phi \approx 10^{-1}$.[58] Determining the volume fraction with an accuracy better than 1%

is difficult[43,59,60], hence the experimentally accessible scaling regime is typically just one decade wide in $\Delta\phi$.

The onset of softening occurs at a strain scale $\gamma^\dagger \sim (p/k) \sim \Delta\phi$. If we take the smallest experimentally accessible value of $\Delta\phi$ to be 10^{-2}, then Hooke's law can (potentially) be observed for strains on the order of 1% and smaller.

To estimate the scales τ^*, γ^*, and $\dot{\gamma}^\dagger$, one must know the microscopic time scale τ_0, which arises from a balance between viscous and elastic forces. Simple dimensional analysis then suggests a time scale on the order of $\eta d/\gamma_s$, where η is the viscosity of the continuous phase, d is a typical bubble size, and γ_s is the surface tension.[61] In dishwasher detergent, for example, viscosities are on the order of 1 mPa·s and surface tensions $\gamma_s \sim 10$ mN/m, while bubble sizes can from 100 μm to 1 cm.[62,63] Hence microscopic time scales fall somewhere in the range $10^{-5} \ldots 10^{-3}$ s. For $\Delta\phi$ on the order 10^{-2}, the time scale $\tau^* \sim \tau_0/(p/k) \sim \tau_0/\Delta\phi$ remains shorter than 0.1 s at accessible values of $\Delta\phi$, while $\dot{\gamma}^\dagger \sim \Delta\phi^2/\tau_0$ can be as low as $0.1\ \mathrm{s}^{-1}$.

We offer a note of caution when considering bounds involving the time scale τ_0. First, experiments find power law relaxation at volume fractions deep in the jammed phase.[64] There is an associated time scale that can be on the order of 1 s depending on sample age, which is significantly longer than our estimates of τ_0 above. This suggests that coarsening and details of the continuous phase flow within thin films and Plateau borders may play an important role – in addition to the strongly non-affine motion associated with proximity to jamming[15,65] – yet neither are incorporated in Durian's bubble model.[4] Second, while we have considered dissipation proportional to the relative velocity of contacting particles, the viscous force law need not be linear. In foams, for example, the dominant source of damping depends sensitively on microscopic details such as the size of the bubbles and the type of surfactant used.[62] Often one finds Bretherton-type damping proportional to (relative) velocity to the power 2/3.[63,66] We anticipate that nonlinear damping would impact the relaxation dynamics[5,67,68] and alter the value of the exponents θ and λ. For sufficiently long times or slow shearing above ϕ_c, however, we expect particles to follow quasistatic trajectories and the differences between various methods of damping to become negligible.

5 Discussion

Using a combination of stress relaxation and flow start-up tests, we have shown that soft solids near jamming are easily driven out of the linear elastic regime. There is, however, a narrow linear elastic window that survives the accumulation of an extensive number of contact changes. This window is bounded from below by viscous dissipation and bounded from above by the onset of strain softening due to plastic dissipation. Close to the transition these two bounds collide and the linear elastic window closes. Hence marginal solids are easily driven into rate-dependent and/or strain softening regimes on at volume fractions and strain scales relevant to the laboratory. Fig. 9 provides a qualitative summary of our results for the case of flow start-up.

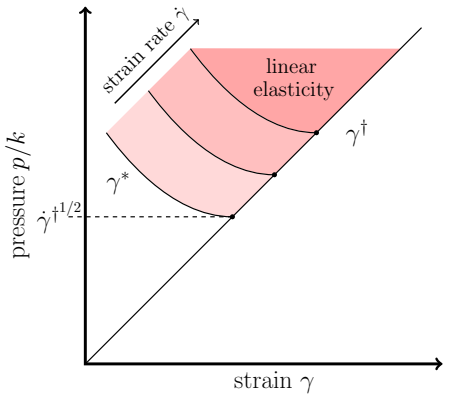

Fig. 9 In a flow start-up test, quasistatic linear response ($G \approx G_0$) occupies a strain window $\gamma^* < \gamma < \gamma^\dagger$ (shaded regions). For smaller strains the response is rate-dependent, with a crossover strain γ^* that depends on both pressure and strain rate. Softening sets in for higher strains, with a crossover $\gamma^\dagger$ that depends only on the pressure. The intersection of the rate-dependent and softening crossovers defines a strain rate $\dot{\gamma}^\dagger$ above which there is no quasistatic linear response, i.e. the shaded region closes.

While our simulations are in two dimensions, we expect the scaling relations we have identified to hold for $D > 2$. To the best of our knowledge, all scaling exponents near jamming that have been measured in both 2D and 3D are the same. There is also numerical evidence that $D = 2$ is the transition's upper critical dimension.[35,55]

Our work provides a bridge between linear elasticity near jamming, viscoelasticity at finite strain rate, and nonlinearity at finite strain amplitude. The measured relaxation modulus G_r is in good agreement with the linear viscoelasticity predicted by Tighe,[15] as well as simulations by Hatano conducted in the unjammed phase.[7] Our findings regarding the crossover to nonlinear strain softening can be compared to several prior studies. The granular experiments of Coulais et al. show softening, although their crossover strain scales differently with the distance to jamming, possibly due to the presence of static friction.[13] The emulsions of Knowlton et al. are more similar to our simulated systems, and do indeed display a crossover strain that is roughly linear in $\Delta\phi$, consistent with our $\gamma^\dagger$.[21] A recent scaling theory by Goodrich et al.[38], by contrast, predicts a crossover strain $\gamma^\dagger \sim \Delta\phi^{3/4}$, which is excluded by our data. Nakayama et al.[36] claim agreement between their numerical data and the theoretical exponent $3/4$, although they note that their data is also compatible with a linear scaling in

$\Delta\phi$. A recent study by Otsuki and Hayakawa[14] also finds a strain scale proportional to $\Delta\phi$ in simulations of large amplitude oscillatory shear at finite frequency. The agreement between the crossover strains in our quasistatic simulations and these oscillatory shear simulations is surprising, as most of the latter results are for frequencies higher than $\dot{\gamma}^\dagger$, where viscous stresses dominate. There are also qualitative differences between the quasistatic shear modulus, which cannot be collapsed to a master curve (Fig. 5), and the storage modulus in oscillatory shear, which can.[14,37] We speculate that there are corresponding microstructural differences between packings in steady state and transient shear,[20] similar to those which produce memory effects.[69]

Soft sphere packings near jamming approach the isostatic state, which also governs the rigidity of closely related materials such as biopolymer and fiber networks.[70–73] It is therefore remarkable to note that, whereas sphere packings soften under strain, quasistatically sheared amorphous networks are strain stiffening beyond a crossover strain that scales as Δz[74], which vanishes more slowly than $\gamma^\dagger \sim \Delta z^2$ in packings. Hence nonlinearity sets in later and with opposite effect in networks.[75] We expect that this difference is attributable to contact changes, which are absent or controlled by slow binding/unbinding processes in networks.

We have demonstrated that softening occurs when the system has accumulated a finite number of contact changes correlated with the system's initial distance from the isostatic state. This establishes an important link between microscopic and bulk response. Yet further work investigating the relationship between microscopic irreversibility, softening, and yielding is needed. The inter-cycle diffusivity in oscillatory shear, for example, jumps at yielding[21,24], but its pressure dependence has not been studied. Shear reversal tests could also provide insight into the connection between jamming and plasticity.

While the onset of softening can be probed with quasistatic simulation methods, rate dependent effects such as the strain scale γ^* should be sensitive to the manner in which energy is dissipated. The dissipative contact forces considered here are most appropriate as a model for foams and emulsions. Hence useful extensions to the present work might consider systems with, e.g., lubrication forces or a thermostat.

6 Acknowledgments

We thank P. Boukany, D. J. Koeze, M. van Hecke, and S. Vasudevan for valuable discussions. ES was supported by the János Bolyai Research Scholarship of the Hungarian Academy of Sciences. JB, DV and BPT acknowledge financial support from the Nederlandse Organisatie voor Wetenschappelijk Onderzoek (Netherlands Organization for Scientific Research, NWO). This work was also sponsored by NWO Exacte Wetenschappen (Physical Sciences) for the use of supercomputer facilities.

References

1 L. D. Landau and E. M. Lifshitz, *Theory of Elasticity*, Butterworth-Heineman, Oxford, 1997.
2 H. A. Barnes and J. F. Hutton, *An Introduction to Rheology*, Elsevier, 1989.
3 F. Bolton and D. Weaire, *Phys. Rev. Lett.*, 1990, **65**, 3449–3451.
4 D. J. Durian, *Phys. Rev. Lett.*, 1995, **75**, 4780–4783.
5 B. P. Tighe, E. Woldhuis, J. J. C. Remmers, W. van Saarloos and M. van Hecke, *Phys. Rev. Lett.*, 2010, **105**, 088303.
6 G. Katgert, B. P. Tighe and M. van Hecke, *Soft Matter*, 2013, **9**, 9739–9746.
7 T. Hatano, *Phys. Rev. E*, 2009, **79**, 050301.
8 J. R. Seth, L. Mohan, C. Locatelli-Champagne, M. Cloitre and R. T. Bonnecaze, *Nat Mater*, 2011, **10**, 838–843.
9 *Handbook of Granular Materials*, ed. S. V. Franklin and M. D. Schattuck, CRC Press, 2015.
10 M. van Hecke, *J. Phys. Cond. Matt.*, 2010, **22**, 033101.
11 A. J. Liu and S. R. Nagel, *Ann. Rev. Cond. Matt. Phys.*, 2010, **1**, 347–369.
12 D. A. Head, *Phys. Rev. Lett.*, 2009, **102**, 138001.
13 C. Coulais, A. Seguin and O. Dauchot, *Phys. Rev. Lett.*, 2014, **113**, 198001.
14 M. Otsuki and H. Hayakawa, *Phys. Rev. E*, 2014, **90**, 042202.
15 B. P. Tighe, *Phys. Rev. Lett.*, 2011, **107**, 158303.
16 L. R. Gómez, A. M. Turner, M. van Hecke and V. Vitelli, *Phys. Rev. Lett.*, 2012, **108**, 058001.
17 S. Ulrich, N. Upadhyaya, B. van Opheusden and V. Vitelli, *PNAS*, 2013, **110**, 20929–20934.
18 S. van den Wildenberg, R. van Loo and M. van Hecke, *Phys. Rev. Lett.*, 2013, **111**, 218003.
19 M. Lundberg, K. Krishan, N. Xu, C. S. O'Hern and M. Dennin, *Phys. Rev. E*, 2008, **77**, 041505.
20 I. Regev, T. Lookman and C. Reichhardt, *Phys. Rev. E*, 2013, **88**, 062401.
21 E. D. Knowlton, D. J. Pine and L. Cipelletti, *Soft Matter*, 2014, **10**, 6931–6940.
22 N. C. Keim and P. E. Arratia, *Phys. Rev. Lett.*, 2014, **112**, 028302.
23 N. C. Keim and P. E. Arratia, *Soft Matter*, 2015, **11**, 1539–1546.
24 T. Kawasaki and L. Berthier, *arXiv:1507.04120*, 2015.
25 G. Combe and J.-N. Roux, *Phys. Rev. Lett.*, 2000, **85**, 3628.

26 E. Lerner, G. Düring and M. Wyart, *Soft Matter*, 2013, **9**, 8252–8263.

27 C. F. Schreck, T. Bertrand, C. S. O'Hern and M. Shattuck, *Phys. Rev. Lett.*, 2011, **107**, 078301.

28 C. F. Schreck, T. Bertrand, C. S. O'Hern and M. D. Shattuck, *arxiv:1306.1961*, 2013.

29 C. F. Schreck, R. S. Hoy, M. D. Shattuck and C. S. O'Hern, *Phys. Rev. E*, 2013, **88**, 052205.

30 C. Schreck, C. O'Hern and M. Shattuck, *Granular Matter*, 2014, **16**, 209–216.

31 T. Bertrand, C. F. Schreck, C. S. O'Hern and M. D. Shattuck, *Phys. Rev. E*, 2014, **89**, 062203.

32 I. Agnolin and J.-N. Roux, *Phys. Rev. E*, 2007, **76**, 061304.

33 M. S. van Deen, J. Simon, Z. Zeravcic, S. Dagois-Bohy, B. P. Tighe and M. van Hecke, *Phys. Rev. E*, 2014, **90**, 020202.

34 C. P. Goodrich, A. J. Liu and S. R. Nagel, *Phys. Rev. Lett.*, 2014, **112**, 049801.

35 C. P. Goodrich, S. Dagois-Bohy, B. P. Tighe, M. van Hecke, A. J. Liu and S. R. Nagel, *Phys. Rev. E*, 2014, **90**, 022138.

36 D. Nakayama, H. Yoshino and F. Zamponi, *arxiv:1512.06544*, 2015.

37 S. Dagois-Bohy, E. Somfai, B. P. Tighe and M. van Hecke, *(in preparation)*, 2014.

38 C. P. Goodrich, A. J. Liu and J. P. Sethna, *arXiv:1510.03469*, 2015.

39 D. J. Evans and G. Morriss, *Statistical Mechanics of Nonequilibrium Liquids*, Cambridge University Press, 2008.

40 D. Vågberg, P. Olsson and S. Teitel, *Phys. Rev. E*, 2011, **83**, 031307.

41 D. Koeze, D. Vågberg, B. Tjoa and B. Tighe, *arXiv:1602.01685*, 2016.

42 C. S. O'Hern, L. E. Silbert, A. J. Liu and S. R. Nagel, *Phys. Rev. E*, 2003, **68**, 011306.

43 G. Katgert and M. van Hecke, *EPL*, 2010, **92**, 34002.

44 S. Dagois-Bohy, B. P. Tighe, J. Simon, S. Henkes and M. van Hecke, *Phys. Rev. Lett.*, 2012, **109**, 095703.

45 R. Ramírez, T. Pöschel, N. V. Brilliantov and T. Schwager, *Phys. Rev. E*, 1999, **60**, 4465.

46 H. P. Zhang and H. A. Makse, *Phys. Rev. E*, 2005, **72**, 011301.

47 W. G. Ellenbroek, E. Somfai, M. van Hecke and W. van Saarloos, *Phys. Rev. Lett.*, 2006, **97**, 258001.

48 M. Wyart, *Annales de Physique*, 2005, **30**, 1.

49 A. Zaccone and E. Scossa-Romano, *Phys. Rev. B*, 2011, **83**, 184205.

50 L. E. Silbert, A. J. Liu and S. R. Nagel, *Phys. Rev. Lett.*, 2005, **95**, 098301.

51 M. Wyart, S. R. Nagel and T. A. Witten, *Europhys. Lett.*, 2005, **72**, 486.

52 A. Tanguy, J. P. Wittmer, F. Leonforte and J.-L. Barrat, *Phys. Rev. B*, 2002, **66**, 174205.

53 S. Alexander, *Phys. Rep*, 1998, **296**, 65–236.

54 C. Maloney, *Phys. Rev. Lett.*, 2006, **97**, 035503.

55 C. P. Goodrich, A. J. Liu and S. R. Nagel, *Phys. Rev. Lett.*, 2012, **109**, 095704.

56 B. P. Tighe, *Phys. Rev. Lett.*, 2012, **109**, 168303.

57 M. Sheinman, C. P. Broedersz and F. C. MacKintosh, *Phys. Rev. E*, 2012, **85**, 021801.

58 C. Zhao, K. Tian and N. Xu, *Phys. Rev. Lett.*, 2011, **106**, 125503.

59 K. W. Desmond, P. J. Young, D. Chen and E. R. Weeks, *Soft Matter*, 2013, **9**, 3424–3436.

60 I. Jorjadze, L.-L. Pontani and J. Brujic, *Phys. Rev. Lett.*, 2013, **110**, 048302.

61 R. Höhler and S. Cohen-Addad, *J. Phys. Cond. Matt.*, 2005, **17**, R1041.

62 M. Le Merrer, R. Lespiat, R. Hohler and S. Cohen-Addad, *Soft Matter*, 2015, **11**, 368–381.

63 G. Katgert, M. E. Möbius and M. van Hecke, *Phys. Rev. Lett.*, 2008, **101**, 058301.

64 S. Cohen-Addad, H. Hoballah and R. Höhler, *Phys. Rev. E*, 1998, **57**, 6897–6901.

65 A. J. Liu, S. Ramaswamy, T. G. Mason, H. Gang and D. A. Weitz, *Phys. Rev. Lett.*, 1996, **76**, 3017–3020.

66 F. P. Bretherton, *J. Fluid Mech.*, 1961, **10**, 166.

67 P. Olsson and S. Teitel, *Phys. Rev. Lett.*, 2007, **99**, 178001.

68 D. Vågberg, P. Olsson and S. Teitel, *Phys. Rev. Lett.*, 2014, **112**, 208303.

69 N. C. Keim, J. D. Paulsen and S. R. Nagel, *Phys. Rev. E*, 2013, **88**, 032306.

70 C. Heussinger and E. Frey, *Phys. Rev. Lett.*, 2006, **96**, 017802.

71 C. Heussinger and E. Frey, *Phys. Rev. Lett.*, 2006, **97**, 105501.

72 C. P. Broedersz, X. Mao, T. C. Lubensky and F. C. MacKintosh, *Nat. Phys.*, 2011, **7**, 983–988.

73 M. Das, D. Quint and J. Schwarz, *PloS One*, 2012, **7**, e35939.

74 M. Wyart, H. Liang, A. Kabla and L. Mahadevan, *Phys. Rev. Lett.*, 2008, **101**, 215501.

75 B. P. Tighe, *Granular Matter*, 2014, **16**, 203–208.